Proceedings of Machine Learning Research vol 245:1–11, 2024 2024 International Conference on Machine Learning and Intelligent Computing

Extended F-expansion Method and Its Application to the Variable-coefficient Fractional Nonlinear Schrödinger Equation

Libin Hao LBHAO678@163.COM
Tianjin University of Technology and Education, Tianjin, 300350, China

Xiaoshan Zhao* XSZHAO678@126.COM
Tianjin University of Technology and Education, Tianjin, 300350, China

Editors: Nianyin Zeng and Ram Bilas Pachori

Abstract

In this paper, under the definition of conformable fractional derivatives, we use the extended F-expansion method and obtain the exact solution of the variable-coefficient factional nonlinear Schrodinger equation (FNLSE), including rational function solutions and Jacobi elliptic function solution. When the mode m of these solutions tends to 1 and 0, the hyperbolic function solution, triangular function solution, and light and dark solitary wave solution are obtained. The correlation diagram of the exact solution is plotted, and the effect of different parameters on the solution structure is deeply analyzed. By selecting a large number of parameters and comparing the graphical analysis of different solutions obtained using this method, we have identified properties related to the nonlinear Schrödinger equation with variable coefficients and summarized relevant theorems.

Keywords: Conformable fractional, Nonlinear Schrödinger equation, Variable-coefficient fractional, Extended F-expand method, Exact solution

1. Introduction

In recent years, the study of fractional nonlinear partial differential equations has penetrated into numerous scientific fields, and nonlinear partial differential equations (PDEs) and fractional partial differential equations (FPDEs) have effectively depicted various physical phenomena (Boyd et al., 2023; Hereman, 2009; Wang et al., 2022), such as deep and shallow water fluctuations, nonlinear optics, chaotic soliton fractal, etc. When describing the dynamical properties of some system models, the fractional nonlinear PDE generalized by the integer order nonlinear partial differential equations can better reflect the actual change law of the system model. The study of the fractional nonlinear Schrödinger equation (FNLSE) and the fractional modified unstable Schrödinger equation (FMUSE) has also sparked significant interest among scientists and has led to successful conclusions in both theoretical and experimental aspects (Wu et al., 2020; Hong, 2023).

The group velocity dispersion of hyperbolic attenuation in optical fiber was demonstrated by Bogatyrev et al. (1991), leading to increased interest from foreign countries (Liu et al., 2019; Chen et al., 2019) in controllable optical solitons and soliton columns in optical communication based on (VC)NLSE. There are numerous methods to solve fractional nonlinear partial differential equations, such as extended direct algebra method (Hong, 2023), Lie group analysis (Sharma and Gupta, 2021), generalized (G'/G) approach Ilhan et al. (2023), the extended tanh-function technique (Zaman et al., 2023) and other effective methods. Solving the exact solution of the nonlinear partial differential equation of the variable coefficients will be beneficial to test the numerical simulations and its qualitative analysis. For the study of fractional nonlinear development equations, we need

R-L fractional derivative, Caputo fractional derivative, conformable fractional derivative, etc (hua Gao et al., 2014; Khalil et al., 2014), and in the study of integer order nonlinear partial differential equation method, also can also be applied to fractional nonlinear partial differential equation, and also is one of the important research trend of nonlinear developmental equation. Due to the intricate nature of solving fractional-order derivatives, and the limitations of each solution method, there is no universal and effective solution method, and only some or more methods can be used to solve a certain class of equations. Therefore, using effective methods for obtaining precise solutions to nonlinear fractional partial differential equations is still one of the topics that need to be studied continuously.

It is well known that (VC) NLSE is widely utilized to explain the characteristics (Liu et al., 2019; Chen et al., 2019) of light waves in nonuniform optical fibers. The fractional-order model holds greater significance than the integer-order model when describing practical problems and studying kinetic properties (Wu et al., 2020; Hashemi and Akgül, 2018).

In this paper, we mainly consider the (VC)FNLSE in the field of nonlinear optics as the (Wu and Dai, 2020),

$$iD_x^{\lambda}H + \frac{1}{2}\alpha(x)D_t^{2\mu}H + \beta(x)H|H|^2 = i\rho(x)H \tag{1}$$

where the complex envelope $H = H(x,t)$ and its derivatives $D_x^{\lambda}H = \frac{\partial^{\lambda}H}{\partial x^{\lambda}}, D_t^{2\mu}H = \frac{\partial^{2\mu}H}{\partial t^{2\mu}}$ with the longitudinal propagation distance x, the delay time t and fractional orders λ and μ. Functions $\alpha(x)$ and $\beta(x)$ are coefficients of the dispersion and Kerr nonlinearity, and function $\rho(x)$ is gain for $\rho(x) > 0$ or loss for $\rho(x) < 0$. If $\lambda = \mu = 1$, Equation 1 is the (VC) NLSE (Liu et al., 2019; Chen et al., 2019).

This paper is primarily structured into the following sections: The initial section, titled "Introduction," provides an overview of the current research status, physical background, and significance of the variable coefficient fractional Schrödinger equation. The second section, titled "Exact Solutions for the Variable Coefficient Spatiotemporal FNLSE," utilizes the extended F-expansion method for the first time to obtain the optical exact solution of this fractional order model, in accordance with the provided fractional order definition (Khalil et al., 2014).The third section, titled "Interpretation of Results," utilizes Maple to draw the three-dimensional graph of the soliton solution obtained through degeneration, contour map, and cross-sectional map under various parameters. Through numerous numerical simulations and graphical analysis, significant new conclusions have been drawn regarding the model. The fourth section, titled "Conclusions," summarizes the findings presented in this article.

2. Exact Solutions For The Variable Coefficient Spatiotemporal FNLSE

For the fractional complex transformation of Equation 1

$$H(x,t) = u(\xi)e^{i\theta}, \xi = M(\frac{x^{\lambda}}{\lambda} - V\frac{t^{\mu}}{\mu}), \theta = C\frac{x^{\lambda}}{\lambda} + \omega\frac{t^{\mu}}{\mu} \tag{2}$$

Substituting Equation 2 into Equation 1 through complex and lengthy fractional order calculations and setting it equal to 0 respectively, the resulting real part is

$$-\mu C + \frac{1}{2}\alpha(M^2V^2u'' - u\omega^2) + \beta u^3 = 0 \tag{3}$$

The imaginary part is

$$Mu^{'} - \alpha MV\omega u^{'} - \rho u = 0 \tag{4}$$

Based on the principle of homogeneous equilibrium, by balancing the highest derivative term $u^{''}$ and the nonlinear term u^3 in Equation 3, we obtain $l = 1$. Therefore, according to the extended F-expansion method (Ozisik et al., 2023; Zhang et al., 2005), we assume that the solution to Equation 4 is

$$u(\xi) = a_0 + a_1 F(\xi) - b_1 F^{-1}(\xi) \tag{5}$$

where a_0, a_1 and b_1 are constants, and $F(\xi)$ satisfies the first elliptic equation $F^{'2}(\xi) = c_0 + c_2 F^2(\xi) + c_4 F^4(\xi)$, where c_0, c_2 and c_4 are constants. Substituting (4) and (5) into Equation 3 and combining the terms with the same power of $F^d(d = 0, 1, 2, 3, 4, 5, 6)$ by maple, and then setting the power coefficient to zero, we can obtain the system of equations involving a_0, a_1, b_1, α and β .

$$-\alpha M^2 V^2 b_1 c_0 - \beta b_1^3 = 0 \tag{6}$$

$$3\beta a_0 b_1^2 = 0 \tag{7}$$

$$Cb_1 + \frac{1}{2}\alpha\omega^2 b_1 - \frac{1}{2}\alpha M^2 V^2 b_1 c_2 - 3\beta a_0^2 b_1 + 3\beta a_1 b_1^2 = 0 \tag{8}$$

$$-ca_0 - \frac{1}{2}\alpha\omega^2 a_0 + \beta a_0^3 - 6\beta a_0 a_1 b_1 = 0 \tag{9}$$

$$-Ca_1 - \frac{1}{2}\alpha\omega^2 a_1 + \frac{1}{2}\alpha M^2 V^2 a_1 c_2 + 3\beta a_0^2 a_1 - 3\beta a_1^2 b_1 = 0 \tag{10}$$

$$3\beta a_0 a_1^2 = 0 \tag{11}$$

$$\alpha M^2 V^2 a_1 c_4 + \beta a_1^3 = 0 \tag{12}$$

Solving the system of Equations 6 $\sim$ 12, the result obtained is

Case 1. The functions α and β are regarded as arbitrary functions of the variable x.

$$a_0 = 0, a_1 = \pm\sqrt{\frac{-\alpha M^2 V^2 c_4}{\beta}}, b_1 = \pm\frac{6c_0}{c_2}\sqrt{\frac{-\alpha M^2 V^2 c_4}{\beta}} \tag{13}$$

Case 2. The functions α and β are regarded as arbitrary functions of the variable x.

$$a_0 = \pm\sqrt{\frac{-\alpha M^2 V^2 c_2}{4\beta}}, a_1 = 0, b_1 = 0 \tag{14}$$

Case 3. The functions α and β are regarded as arbitrary functions of the variable x.

$$a_0 = \pm\sqrt{\frac{\alpha\omega^2 + 2C}{2\beta}}, a_1 = 0, b_1 = 0 \tag{15}$$

According to Equations 2, 5 and ODE and Jacobi elliptic function (Zhang et al., 2005), we have several solutions to the following Equation 1

Solution 1. $F(\xi) = sn\xi, c_0 = 1, c_2 = -(1+m^2), c_4 = m^2,$

$$H_{11}(x,t) = (\pm\sqrt{\frac{-\alpha M^2V^2m^2}{\beta}}sn\xi \pm \frac{6}{1+m^2}\sqrt{\frac{-\alpha M^2V^2m^2}{\beta}}ns\xi)e^{i(C\frac{x^\lambda}{\lambda}+\omega\frac{t^\mu}{\mu})} \tag{16}$$

when $m \to 1$, bright soliton solution is denoted as

$$H_{11}^{'}(x,t) = (\pm\sqrt{\frac{-\alpha M^2V^2}{\beta}}\tanh\xi \pm 3\sqrt{\frac{-\alpha M^2V^2}{\beta}}\coth\xi)e^{i(C\frac{x^\lambda}{\lambda}+\omega\frac{t^\mu}{\mu})} \tag{17}$$

Solution 2. $F(\xi) = cn\xi, c_0 = 1-m^2, c_2 = 2m^2-1, c_4 = -m^2,$

$$H_{21}(x,t) = (\pm\sqrt{\frac{\alpha M^2V^2m^2}{\beta}}cn\xi \pm \frac{6(1-m^2)}{2m^2-1}\sqrt{\frac{\alpha M^2V^2m^2}{\beta}}nc\xi)e^{i(C\frac{x^\lambda}{\lambda}+\omega\frac{t^\mu}{\mu})} \tag{18}$$

when $m \to 1$, kink wave solution is denoted as

$$H_{21}^{'}(x,t) = (\pm\sqrt{\frac{\alpha M^2V^2}{\beta}}\mathrm{sech}\xi)e^{i(C\frac{x^\lambda}{\lambda}+\omega\frac{t^\mu}{\mu})} \tag{19}$$

Solution 3. $F(\xi) = ds\xi, c_0 = -m^2(1-m^2), c_2 = 2m^2-1, c_4 = 1,$

$$H_{31}(x,t) = (\pm\sqrt{\frac{-\alpha M^2V^2}{\beta}}\frac{dn\xi}{sn\xi} \pm \frac{6m^2(1-m^2)}{2m^2-1}\sqrt{\frac{-\alpha M^2V^2}{\beta}}\frac{sn\xi}{dn\xi})e^{i(C\frac{x^\lambda}{\lambda}+\omega\frac{t^\mu}{\mu})} \tag{20}$$

when $m \to 1$, the soliton solution for the bright-dark wave is denoted as

$$H_{31}^{'}(x,t) = (\pm\sqrt{\frac{-\alpha M^2V^2}{\beta}}\coth\xi)e^{i(C\frac{x^\lambda}{\lambda}+\omega\frac{t^\mu}{\mu})} \tag{21}$$

Solution 4. $F(\xi) = ns\xi, c_0 = m^2, c_2 = -(1+m^2), c_4 = 1,$

$$H_{41}(x,t) = (\pm\sqrt{\frac{-\alpha M^2V^2}{\beta}}ns\xi \pm \frac{6m^2}{1+m^2}\sqrt{\frac{-\alpha M^2V^2}{\beta}}sn\xi)e^{i(C\frac{x^\lambda}{\lambda}+\omega\frac{t^\mu}{\mu})} \tag{22}$$

when $m \to 0$, the periodic soliton solution is

$$H_{41}^{'}(x,t) = (\pm\sqrt{\frac{-\alpha M^2V^2}{\beta}}\csc\xi)e^{i(C\frac{x^\lambda}{\lambda}+\omega\frac{t^\mu}{\mu})} \tag{23}$$

Solution 5. $F(\xi) = nc\xi, c_0 = -m^2, c_2 = 2m^2-1, c_4 = 1-m^2,$

$$H_{51}(x,t) = (\pm\sqrt{\frac{-\alpha M^2V^2(m^2-1)}{\beta}}nc\xi \pm \frac{6m^2}{2m^2-1}\sqrt{\frac{\alpha M^2V^2(m^2-1)}{\beta}}cn\xi)e^{i(C\frac{x^\lambda}{\lambda}+\omega\frac{t^\mu}{\mu})} \tag{24}$$

when $m \to 0$, the periodic soliton solution is

$$H_{51}^{'}(x,t) = (\pm\sqrt{\frac{-\alpha M^2 V^2}{\beta}}\sec\xi)e^{i(C\frac{x^\lambda}{\lambda}+\omega\frac{t^\mu}{\mu})} \tag{25}$$

Solution 6. $F(\xi) = cn\xi, c_0 = 1-m^2, c_2 = 2m^2-1, c_4 = -m^2,$

$$H_{61}(x,t) = (\pm\sqrt{\frac{-\alpha M^2 V^2(2m^2-1)}{4\beta}})e^{i(C\frac{x^\lambda}{\lambda}+\omega\frac{t^\mu}{\mu})} \tag{26}$$

Solution 7. $F(\xi) = cn\xi, c_0 = 1-m^2, c_2 = 2m^2-1, c_4 = -m^2,$

$$H_{71}(x,t) = (\pm\sqrt{\frac{\alpha\omega^2+2C}{2\beta}})e^{i(C\frac{x^\lambda}{\lambda}+\omega\frac{t^\mu}{\mu})} \tag{27}$$

Various solutions are provided based on the calculation results, and additional repeat types are not included in this list. These obtained solutions are new exact solutions for the variable coefficient nonlinear Schrödinger equation, demonstrating the effectiveness of this method. The results are used to generate three-dimensional graphs for Solution 1 to Solution 5, corresponding contour maps, and sectional graphs obtained under different parameters. The configuration of Solution 6 and Solution 7 depends on the functions α and β.

3. Interpretation Of Results

The particular arrangement of the solution reflects the characteristics of wave propagation within the medium as described by the optical system. The discussion primarily focused on the analysis of two perspectives: the impact of the variation of the fractional order parameters λ and μ on the solution structure while keeping functions α and β unchanged, and the influence of the variation of functions α and β on the solution structure while keeping fractional order parameters λ and μ unchanged. Based on the analysis of the exact solution $\left|H_i^{'}(x,t)\right|^2$ obtained from the degenerate Equation 1 in Figures 1 and 2, when the functions α and β remain unchanged, the variations of λ and μ in (a) and (d) in Figures 1 and 2 both indicate that the waveform structure of the corresponding equation's soliton solution has hardly undergone essential changes. (b), (e), (c) and (f) in Figures 1 and 2 indicate that the direction of wave motion has not changed, and the wave peaks have not shifted in position, demonstrating periodic oscillations. We observe that the soliton solutions (17), (19), and (21) are all composed of hyperbolic functions, which reflect the optical properties of the wave propagation described by the corresponding model (1). In Figure 3, the waveforms of the soliton solutions of the respective equations undergo significant changes as λ and μ vary, while the functions α and β remain unchanged. (a) and (d) in Figure 3 exhibit significant changes in the waveform structure of the soliton solutions. (b), (e), (c), and (f) in Figure 3 demonstrate significant changes in the direction of wave propagation, along with noticeable shifts in the peak positions of the waves, while still maintaining periodic oscillations. Both soliton solutions (23) and (25) involve trigonometric functions, which correspond to the optical characteristics of the wave propagation as described by the respective model (1). When the fractional order parameters λ and μ remain unchanged, and the functions α and β change in Figures 1, 2, and 3, both Figures (c) and (f) indicate

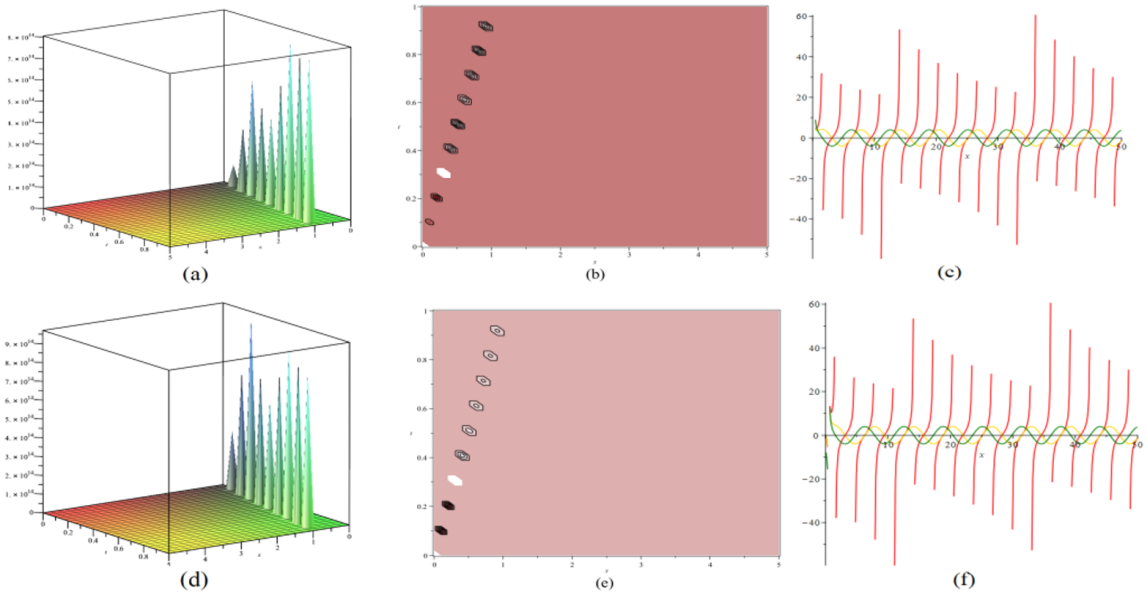

Figure 1: Figures (a) and (d) depict three-dimensional representations of the solution $\left|H_{11}^{'}(x,t)\right|^2$, with each graph corresponding to the parameters $\alpha(x) = -\sin^2(x), \lambda = 1/2, \mu = 1/2, M = 1, \beta(x) = \cos^2(x), V = 1, C = 1, \omega = -5$ and $\alpha(x) = -\sin^2(x), \lambda = 1, \mu = 1, \beta(x) = \cos^2(x),, V = 1, M = 1, \omega = -5, C = 1$, respectively. Figures (b) and (e) depict contour plots representing the respective parameters. Figure (c) depicts the cross-sectional view of $\left|H_{11}^{'}(x,t)\right|^2$ under different parameters at $t = 1/2$. The red line represents the value of $M = 1, \alpha(x) = -\sin^2(x), \lambda = 1/2, \omega = -5, \mu = 1/2, \beta(x) = \cos^2(x), C = 1, V = 1$, the yellow line represents the value of $\alpha(x) = -\cos^2(x), \lambda = 1/2, C = 1, \mu = 1/2, \beta(x) = \cot^2(x), M = 1, V = 1, \omega = -5$, and the green line represents the value of $V = 1, \alpha(x) = -\sin^2(x), \lambda = 1/2, \mu = 1/2, \beta(x) = \tan^2(x), M = 1, C = 1, \omega = -5$. Figure (f) depicts the cross-sectional view of $\left|H_{11}^{'}(x,t)\right|^2$ under different parameters at $t = 1/2$. The red line represents the value of $\alpha(x) = -\sin^2(x), M = 1, \lambda = 1, \mu = 1, \beta(x) = \cos^2(x), \omega = -5, V = 1, C = 1$, the yellow line represents the value of $\alpha(x) = -\cos^2(x), \lambda = 1, \mu = 1, \beta(x) = \cot^2(x), M = 1, V = 1, \omega = -5, C = 1$, and the green line represents the value of $\alpha(x) = -\sin^2(x), \lambda = 1, \mu = 1, \beta(x) = \tan^2(x), M = 1, C = 1, \omega = -5, V = 1$.

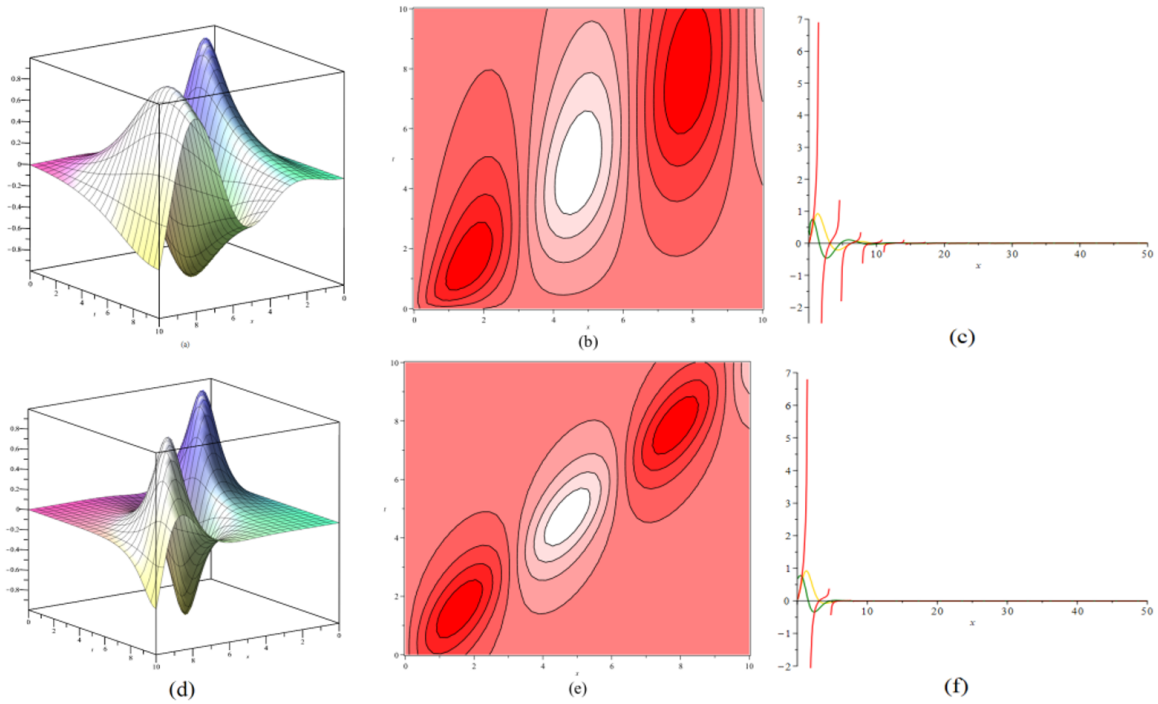

Figure 2: Figures (a) and (d) depict three-dimensional representations of the solution $\left|H_{21}^{'}(x,t)\right|^2$, with each graph corresponding to the parameters $\alpha(x) = \cos^2(x), \lambda = 1/2, \mu = 1/2, \beta(x) = \cot^2(x), M = 1, V = 1, C = 1, \omega = -1$ and $\alpha(x) = \cos^2(x), \lambda = 1, \mu = 1, \beta(x) = \cot^2(x), M = 1, V = 1, C = 1, \omega = -1$, respectively. Figures (b) and (e) depict contour plots representing the respective parameters. Figure (c) depicts the cross-sectional view of $\left|H_{21}^{'}(x,t)\right|^2$ under different parameters at $t = 1/2$. The red line represents the value of $\alpha(x) = -\sin^2(x), \lambda = 1/2, \mu = 1/2, \beta(x) = \cos^2(x), M = 1, V = 1, C = 1, \omega = -1$, yellow line represents the value of $\alpha(x) = -\cos^2(x), \lambda = 1/2, \mu = 1/2, \beta(x) = \cot^2(x), M = 1, V = 1, C = 1, \omega = -1$ and green line represents the value of $\alpha(x) = -\sin^2(x), \lambda = 1/2, \mu = 1/2, \beta(x) = \tan^2(x), M = 1, V = 1, C = 1, \omega = -1$. (f) depicts the cross-sectional view of $\left|H_{21}^{'}(x,t)\right|^2$ under different parameters at $t = 1/2$. The red line represents the value of $\alpha(x) = -\sin^2(x), \lambda = 1, \mu = 1, \beta(x) = \cos^2(x), M = 1, V = 1, C = 1, \omega = -1$, the yellow line represents the value of $\alpha(x) = -\cos^2(x), \lambda = 1, \mu = 1, \beta(x) = \cot^2(x), M = 1, V = 1, C = 1, \omega = -1$, and the green line represents the value of $\alpha(x) = -\sin^2(x), \lambda = 1, \mu = 1, \beta(x) = \tan^2(x), M = 1, V = 1, C = 1, \omega = -1$.

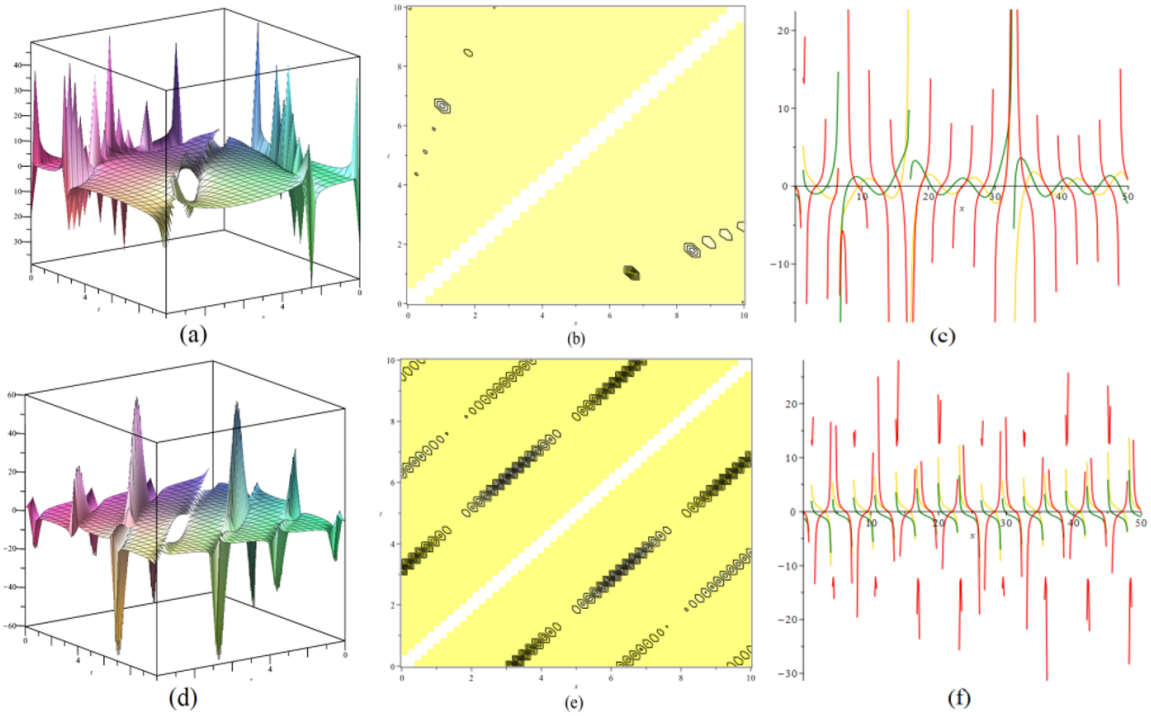

Figure 3: Figures (a) and (d) depict three-dimensional representations of the solution $\left|H_{41}^{'}(x,t)\right|^2$, with each graph corresponding to the parameters $\alpha(x) = 4\sin^2(x), \lambda = 1/2, \mu = 1/2, \beta(x) = \cos^2(x), M = 1, V = 1, C = 1, \omega = -1$ and $\alpha(x) = 4\sin^2(x), \lambda = 1, \mu = 1, \beta(x) = \cos^2(x), M = 1, V = 1, C = 1, \omega = -1$, respectively. Figures (b) and (e) depict contour plots representing the respective parameters. Figure (c) depicts the cross-sectional view of $\left|H_{41}^{'}(x,t)\right|^2$ under different parameters at $t = 1$. The red line represents the value of $\alpha(x) = 4\sin^2(x), \lambda = 1/2, \mu = 1/2, \beta(x) = \cos^2(x), M = 1, V = 1, , \omega = -1, C = 1$, yellow line represents the value of $\alpha(x) = 4\cos^2(x), \lambda = 1/2, \mu = 1/2, \beta(x) = \cot^2(x), M = 1, C = 1, \omega = -1, V = 1$ and green line represents the value of $\alpha(x) = 4\sin^2(x), \lambda = 1/2, C = 1, \omega = -1, \mu = 1/2, \beta(x) = \tan^2(x), M = 1, , V = 1$. (f) depicts the cross-sectional view of $\left|H_{41}^{'}(x,t)\right|^2$ under different parameters at $t = 1$. The red line represents the value of $\alpha(x) = 4\sin^2(x), \lambda = 1, \mu = 1, \beta(x) = \cos^2(x), M = 1, V = 1, C = 1, \omega = -1$, the yellow line represents the value of $\alpha(x) = 4\cos^2(x), \lambda = 1, \mu = 1, \beta(x) = \cot^2(x), M = 1, V = 1, C = 1, \omega = -1$, and the green line represents the value of $\alpha(x) = 4\sin^2(x), \lambda = 1, \mu = 1, \beta(x) = \tan^2(x), M = 1, V = 1, C = 1, \omega = -1$.

that when the function $\frac{\alpha(x)}{\beta(x)} = \sin(x)$ (yellow line), the resulting waveform structure of the solution at the same moment t is almost identical to when the function $\frac{\alpha(x)}{\beta(x)} = \cos(x)$ (green line). However, when the function $\frac{\alpha(x)}{\beta(x)} = \tan(x)$ (red line), the waveform structure of the solution undergoes a significant change. Other solutions of the same type have been verified and are consistent with the relevant conclusions. In summary, we have come to the following theorem:

Theorem 4.1. When the functions $\alpha(x)$ and $\beta(x)$ remain unchanged, the structure of the equation's solutions depends on the type of soliton solution obtained through degeneracy, as the value of the fractional-order derivative λ increases from 1/2 to 1 and μ increases from 1/2 to 1. When the function $\alpha(x)$ and $\beta(x)$ is hyperbolic, the structure of the equation's solutions undergoes almost no significant changes. When the function $\alpha(x)$ and $\beta(x)$ is trigonometric, the structure of the equation's solutions undergoes significant changes. When the fractional order parameters λ and μ remain unchanged, the waveform structure of the solution undergoes a significant change in the function $\tan(x)$.

4. Conclusions

In conclusion, based on the definition of the conformable fractional-order derivative, this paper utilizes the extended F-expansion method to obtain exact solutions for the (VC) FNLSE. We have obtained additional exact solutions for this model, including Hyperbolic function solutions and trigonometric periodic solutions. To enhance our comprehension of the physical phenomena in this model and investigate the propagation characteristics of optical solitons, we have created three-dimensional contour and cross-sectional graphs of the exact solutions. It contributes to advancing our understanding of the optical properties of wave propagation, as described by the fractional-order model. It can be observed that when α and β are constants, these solutions can be transformed into solutions of the (CC) FNLSE. Due to the intricate nature of solving fractional-order derivatives, the extended F-expansion method is only capable of offering partial solutions for this model. Through graphical analysis, we can visually represent the optical properties of wave propagation described by this model, draw relevant conclusions and demonstrate that this is an effective approach for obtaining exact solutions of (VC) FPDEs.

Acknowledgments

This work was supported by the National Natural Science Foundation of China (No.12001404). This work was supported by Tianjin University Science and Technology Development Fund /2023KJ196.

References

V.A. Bogatyrev, M.M. Bubnov, E.M. Dianov, A.S. Kurkov, P.V. Mamyshev, A.M. Prokhorov, S.D. Rumyantsev, V.A. Semenov, S.L. Semenov, A.A. Sysoliatin, S.V. Chernikov, A.N. Gur'yanov, G.G. Devyatykh, and S.I. Miroshnichenko. A single-mode fiber with chromatic dispersion varying along the length. *Journal of Lightwave Technology*, 9(5):561–566, 1991. doi: 10.1109/50.79530.

Robert W. Boyd, Alexander L. Gaeta, and Enno Giese. *Nonlinear Optics*, pages 1097–1110. Springer International Publishing, Cham, 2023. ISBN 978-3-030-73893-8. doi: 10.1007/978-3-030-73893-8_76.

Shao-Jiang Chen, Jia-Ni Lin, and Yue-Yue Wang. Soliton solutions and their stabilities of three $(2+1)$-dimensional pt-symmetric nonlinear schrödinger equations with higher-order diffraction and nonlinearities. *Optik*, 194:162753, 2019. doi: 10.1016/j.ijleo.2019.04.099.

M.S. Hashemi and Ali Akgül. Solitary wave solutions of time–space nonlinear fractional schrödinger's equation: Two analytical approaches. *Journal of Computational and Applied Mathematics*, 339:147–160, 2018. doi: 10.1016/j.cam.2017.11.013. Modern Fractional Dynamic Systems and Applications, MFDSA 2017.

Willy Hereman. *Shallow Water Waves and Solitary Waves*, pages 8112–8125. Springer New York, New York, NY, 2009. doi: 10.1007/978-0-387-30440-3_480.

Baojian Hong. Exact solutions for the conformable fractional coupled nonlinear schrödinger equations with variable coefficients. *Journal of Low Frequency Noise, Vibration and Active Control*, 42(2):628–641, 2023. doi: 10.1177/14613484221135478.

Guang hua Gao, Zhi zhong Sun, and Hong wei Zhang. A new fractional numerical differentiation formula to approximate the caputo fractional derivative and its applications. *Journal of Computational Physics*, 259:33–50, 2014. doi: 10.1016/j.jcp.2013.11.017.

Onur Alp Ilhan, Haci Mehmet Baskonus, M. Nurul Islam, M. Ali Akbar, and Danyal Soybaş. Stable soliton solutions to the time fractional evolution equations in mathematical physics via the new generalized g/g-expansion method. *International Journal of Nonlinear Sciences and Numerical Simulation*, 24(1):185–200, 2023. doi: 10.1515/ijnsns-2020-0153.

R. Khalil, M. Al Horani, A. Yousef, and M. Sababheh. A new definition of fractional derivative. *Journal of Computational and Applied Mathematics*, 264:65–70, 2014. doi: 10.1016/j.cam.2014.01.002.

Suzhi Liu, Qin Zhou, Anjan Biswas, and Wenjun Liu. Phase-shift controlling of three solitons in dispersion-decreasing fibers. *Nonlinear Dynamics*, 98, 10 2019. doi: 10.1007/s11071-019-05200-5.

Muslum Ozisik, Aydin Secer, and Mustafa Bayram. On solitary wave solutions for the extended nonlinear schrödinger equation via the modified f-expansion method. *Optical and Quantum Electronics*, 55, 01 2023. doi: 10.1007/s11082-022-04476-z.

Manjeet Sharma and Rajesh Gupta. Symmetry reduction, conservation laws and power series solution of time-fractional variable coefficient caudrey–dodd–gibbon–sawada–kotera equation. *Mathematical Sciences*, 17, 10 2021. doi: 10.1007/s40096-021-00443-z.

Qing Wang, Lingling Zhang, Boris A. Malomed, Dumitru Mihalache, and Liangwei Zeng. Transformation of multipole and vortex solitons in the nonlocal nonlinear fractional schrödinger equation by means of lévy-index management. *Chaos, Solitons & Fractals*, 157:111995, 2022. doi: 10.1016/j.chaos.2022.111995.

Gang-Zhou Wu and Chao-Qing Dai. Nonautonomous soliton solutions of variable-coefficient fractional nonlinear schrödinger equation. *Applied Mathematics Letters*, 106:106365, 2020. doi: 10.1016/j.aml.2020.106365.

Gang-Zhou Wu, Li-Jun Yu, and Yue-Yue Wang. Fractional optical solitons of the space-time fractional nonlinear schrödinger equation. *Optik*, 207:164405, 2020. ISSN 0030-4026. doi: 10.1016/j.ijleo.2020.164405.

U.H.M. Zaman, Mohammad Asif Arefin, M. Ali Akbar, and M. Hafiz Uddin. Utilizing the extended tanh-function technique to scrutinize fractional order nonlinear partial differential equations. *Partial Differential Equations in Applied Mathematics*, 8:100563, 2023. ISSN 2666-8181. doi: 10.1016/j.padiff.2023.100563.

Jie-Fang Zhang, Chao-Qing Dai, Qin Yang, and Jia-Min Zhu. Variable-coefficient f-expansion method and its application to nonlinear schrödinger equation. *Optics Communications*, 252(4): 408–421, 2005. ISSN 0030-4018. doi: 10.1016/j.optcom.2005.04.043.